

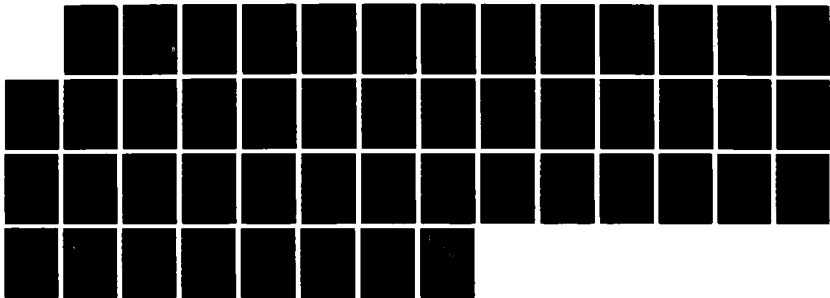
ND-REI93 073

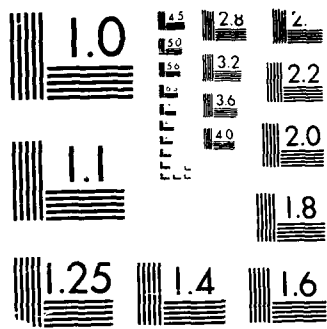
INTERACTION BETWEEN LUNG MECHANICS AND GAS EXCHANGE BY 171
LOW VOLUME HIGH FR. (U) BRIGHAM AND WOMEN'S HOSPITAL
BOSTON MA J M DRAZEN ET AL. 21 NOV 84 DAND17-82-C-2210

UNCLASSIFIED

F/G 6/5

ML





MICROCOPY RESOLUTION TEST CHART
ANSI AND ISO STANDARDS 1963-A

AD-A193 073

DTIC FILE COPY

AD _____

Interaction between Lung Mechanics and Gas Exchange by Low Volume High Frequency Pulmonary Ventilation in Patients with Respiratory Failure

Annual Summary Report

Jeffrey M. Drazen, M.D., Phillip Drinker, Ph.D., Thomas Rossing, M.D.
Julian Solway, M.D., Roger D. Kamm, Ph.D., Ishmail Dreshai, M.D.
and Rayhana Akhavan

November 21, 1984

Supported by

U.S. ARMY MEDICAL RESEARCH AND DEVELOPMENT COMMAND
Fort Detrick, Frederick, Maryland 21701-5012

Contract No. DAMD17-82-C-2210

Brigham and Women's Hospital
75 Francis Street
Boston, Massachusetts 02115

DOD Distribution Statement

DTIC
SELECTED
MAR 28 1988
S E D

Approved for public release; distribution unlimited

The findings in this report are not to be construed as an official Department of the Army position unless so designated by other authorized documents.

88 8 22 095

REPORT DOCUMENTATION PAGE

Form Approved
OMB No. 0704-0188

1a. REPORT SECURITY CLASSIFICATION Unclassified		1b. RESTRICTIVE MARKINGS	
2a. SECURITY CLASSIFICATION AUTHORITY		3. DISTRIBUTION / AVAILABILITY OF REPORT Approved for public release; distribution unlimited	
2b. DECLASSIFICATION / DOWNGRADING SCHEDULE		4. PERFORMING ORGANIZATION REPORT NUMBER(S)	
4. PERFORMING ORGANIZATION REPORT NUMBER(S)		5. MONITORING ORGANIZATION REPORT NUMBER(S)	
6a. NAME OF PERFORMING ORGANIZATION Brigham and Women's Hospital	6b. OFFICE SYMBOL (if applicable)	7a. NAME OF MONITORING ORGANIZATION	
6c. ADDRESS (City, State, and ZIP Code) 75 Francis Street Boston, MA 02115		7b. ADDRESS (City, State, and ZIP Code)	
8a. NAME OF FUNDING / SPONSORING ORGANIZATION U.S. Army Medical Research & Development Command	8b. OFFICE SYMBOL (if applicable)	9. PROCUREMENT INSTRUMENT IDENTIFICATION NUMBER Contract No. DAMD17-82-C-2210	
8c. ADDRESS (City, State, and ZIP Code) Fort Detrick, Frederick, Maryland 21701-5012		10. SOURCE OF FUNDING NUMBERS	
		PROGRAM ELEMENT NO. 62734A	PROJECT NO. 3M1- 62734A875
		TASK NO. CC	WORK UNIT ACCESSION NO. 336
11. TITLE (Include Security Classification) Interaction between Lung Mechanics and Gas Exchange by Low Volume High Frequency Pulmonary Ventilation in Patients with Respiratory Failure			
12. PERSONAL AUTHOR(S) Jeffrey M. Drazen, M.D.; Phillip Drinker, Ph.D.; Thomas Rossing, M.D.; Julian Solway, M.D.; Roger D. Kamm, Ph.D.; Ismail Dreshaj, M.D.; Rayhana Akhavan			
13a. TYPE OF REPORT Annual Report	13b. TIME COVERED FROM 83/10/1 TO 84/9/30	14. DATE OF REPORT (Year, Month, Day) 1984 November 21	15. PAGE COUNT 45
16. SUPPLEMENTARY NOTATION			
17. COSATI CODES		18. SUBJECT TERMS (Continue on reverse if necessary and identify by block number)	
FIELD	GROUP	High Frequency Ventilation	
15	06	Mechanical Ventilation	
06	11		
19. ABSTRACT (Continue on reverse if necessary and identify by block number)			
<p>The factors influencing both dynamic hyperinflation and gas transport under the condition of low volume high frequency pulmonary ventilation (HFV) were examined. In the former area we measured gas transport and dynamic lung volumes in tracheostomized human subjects simultaneously in order to help determine the mechanism(s) responsible for gas trapping. We found that application of a fixed tidal volume (~50-100 ml) over a range of frequencies from 0.5-20 Hz resulted in increased gas transport efficiency until a critical frequency was reached; above this frequency no further increase in alveolar ventilation was achieved. In contrast, mean lung volume (dynamic functional residual capacity) increased only above a critical frequency.</p> <p>These findings were compared using a variety of electrical analog models including one which incorporated airflow limitation; our findings suggest that airflow limitation mediates dynamic hyper-inflation. We also made measurements of gas transport during oscillatory flow in a hardware model which incorporated branching airways. We cast our results in the form of</p>			
20. DISTRIBUTION / AVAILABILITY OF ABSTRACT <input type="checkbox"/> UNCLASSIFIED/UNLIMITED <input checked="" type="checkbox"/> SAME AS RPT <input type="checkbox"/> DTIC USE ONLY		21. ABSTRACT SECURITY CLASSIFICATION Unclassified	
22a. NAME OF RESPONSIBLE INDIVIDUAL Mrs. Virginia M. Miller		22b. TELEPHONE (Include Area Code) 301/663-7325	22c. OFFICE SYMBOL SGRD-RMI-S

19. Abstract (Continued)

an effective axial diffusion coefficient where

$$D_{eff} = (K + 0.5V_T^{1.66}f^{0.94})\text{cm}^2/\text{sec}$$

is the molecular diffusivity, V_T the stroke volume, and f the oscillatory frequency. At low frequency our results are similar to those of Scherer and co-workers. At higher frequencies, frequency rather than flow rate per se becomes an important variable.

Accession For	
NTIS GRA&I	<input checked="" type="checkbox"/>
DTIC TAB	<input type="checkbox"/>
Unannounced	<input type="checkbox"/>
Justification	
By _____	
Distribution/	
Availability Codes	
Dist	Avail and/or Special
A-1	



TABLE OF CONTENTS

Abstract	3
Foreword	4
I. Introduction	5
II. Methods	6
A. Experiments in Patients	6
B. Computational Model	7
C. Gas Transport in Hardware Models	8
III. Results	11
A. Experiments in Patients	11
B. Predictions of Transistor Model	11
C. Gas Transport Model Experiments	12
IV. Discussion	13
A. Patient Studies	13
B. Hardware Model Studies	15
V. Military Significance	21
VI. References	22
VII. Glossary	24
VIII. Figures	26
A. Figure 1	
B. Figure 2	
C. Figure 3	
D. Figure 4	
E. Figure 5	
F. Figure 6	
G. Figure 7	
H. Figure 8	
I. Figure 9	
IX. Table I	44
X. Distribution List	45

about

ABSTRACT

The factors influencing both dynamic hyperinflation and gas transport under the condition of low volume high frequency pulmonary ventilation (HFV)* were examined. In the former area we measured gas transport and dynamic lung volumes in tracheostomized human subjects simultaneously in order to help determine the mechanism(s) responsible for gas trapping. We found that application of a fixed tidal volume (50-100 ml) over a range of frequencies from 0.5-20 Hz resulted in increased gas transport efficiency until a critical frequency was reached; above this frequency no further increase in alveolar ventilation was achieved. In contrast, mean lung volume (dynamic functional residual capacity) increased only above a critical frequency. These findings were compared using a variety of electrical analog models including one which incorporated airflow limitation; our findings suggest that airflow limitation mediates dynamic hyper-inflation. We also made measurements of gas transport during oscillatory flow in a hardware model which incorporated branching airways. We cast our results in the form of an effective axial diffusion coefficient where

$$D_{\text{eff}} = (K + 0.5V_T^{1.66}f^{0.94}) \text{cm}^2/\text{sec}$$

is the molecular diffusivity, V_T the stroke volume, and f the oscillatory frequency. At low frequency our results are similar to those of Scherer and co-workers. At higher frequencies, frequency rather than flow rate per se becomes an important variable.

* abbreviations and their definitions are listed in the glossary (page 23)

FOREWORD

For the protection of human subjects the investigator(s) have adhered to the policies of applicable Federal Law 45CFR46.

Citations of commercial organizations and trade names in this report do not constitute an official Department of the Army endorsement or approval of the products or services of these organizations.

I. INTRODUCTION

High frequency low tidal volume oscillatory ventilation (HFV) may be of value as a method of respiratory support for combat casualties. However it seemed possible that hyper-inflation of the lung could occur during application of HFV and that this hyper-inflation could limit the utility of the ventilatory mode. Further since basic information about the mechanisms controlling gas transport during HFV was not known, studies were conducted in a hardware model to better understand how gas transport is effected in such circumstances.

Recent studies have demonstrated that dynamic hyperinflation may occur in animals (1) or in patients (2) during low tidal volume HFV. In these studies, when relatively large tidal volumes (~100 ml) were applied at relatively high frequencies (~15 Hz or greater), the mean pressure within the alveoli was found to exceed the mean airway opening pressure, sometimes by as much as 30 cm H₂O. Simon et al (1) attributed this phenomenon, which they observed in healthy dogs, to either erroneous pressure estimation at the airway opening due to convective accelerative pressure loss, or to asymmetry of airways impedance during inspiration and expiration, as a potential explanation for this phenomenon.

In cineradiobronchograms during HFV in dogs (3), we have noted nonsinusoidal diameter variations about the mean airway diameter in a variety of central airways during sinusoidal forcing. In addition, pressure tracings from measurement at the airway opening in patients (4) show similar asymmetry, with larger negative deflections than positive deflections from the mean. These results strongly suggest that asymmetry of respiratory impedance may be important in creating disparate alveolar and airway opening mean pressures.

The present study in human subjects was undertaken to address the mechanisms responsible for this asymmetry. We measured simultaneous gas exchange and dynamic hyperinflation in patients, and compared these results with predictions from a simple computational model. We found that expiratory flow limitation, rather than fixed asymmetric or variable asymmetric resistance, best accounts for the experimental data reported here.

Since hyper-inflation did not occur at all frequency and tidal volume combinations studied, it seemed reasonable to further examine the basic physics of gas transport when small tidal volumes were used.

Several attempts have been made to simulate the exchange of gases through the respiratory system due to transport of a diffusive nature (5,6) and due to direct alveolar ventilation (7). Of these, diffusive transport models are most appropriate for very small tidal volumes. Although such models are useful in predicting some of the observed frequency and tidal volume dependence of experimental data, they are deficient in that they

are based merely on reasonable estimates of the actual rate of dispersion within the lung rather than analyses or experiments in which the conditions of HFV are appropriately modeled.

Several groups have recently conducted experiments to help elucidate and quantify the mechanisms of transport under conditions of small volume, high frequency oscillation. Tarbell et al (8) and Azhar and Tarbell (9) have measured the dispersion of a bolus of liquid dye in a five-generation model. In Tarbell's experiments, oscillations are imposed until the bolus spreads over the entire network. The fluid is then allowed to drain and the distribution of dye is measured as a function of the volume of fluid expelled. Measurements of effective axial diffusivity are determined from the volume variance of the concentration distribution and therefore represent an overall network dispersion coefficient.

Some preliminary results have recently been reported for oscillatory gas flow in bifurcating systems of similar systems of similar geometry (10,11). While these experiments for gases and liquids all measure the rate at which axial dispersion occurs in branching tubes, there exist some important differences as to the rate of molecular diffusion in gas transport. The results reported so far, however, do not permit an assessment of the influence of molecular diffusion.

The primary objective of these experiments was to obtain correlations which can be used in simulations of gas exchange in the lung by HFV which occurs over all airway branches (5,7). As described later, these results are generally applicable to airways from generations 5-13 of the Weibel (12) morphometric model of the human lung. In addition, however, these results, in combination with those of other investigators, help us to characterize better the flow and gas transport processes and to address questions relating to the physical mechanisms effecting gas transport.

II. METHODS

A. Experiments in Patients

Four patients with chronic respiratory insufficiency served as subjects for the study; patients were studied in the supine position. Each required long-term mechanical ventilatory support; their characteristics are provided in Table 1. Informed consent was obtained from each patient or his/her guardian.

Changes in lung volume were assessed with a RespiTrace impedance plethysmograph. RespiTrace belts were positioned around the abdomen and around the chest; relative gains were adjusted so that changes in the sum of the two signals were proportional to changes in lung volume. Calibration of the RespiTrace volume signal was performed by delivering breaths of known volume from a large syringe.

The apparatus used to deliver HFV was similar to that referred to previously (13). The outflow rate of a high impedance bias flow (mean rate 30 L/min) was servo-controlled to maintain mean airway pressure at the airway opening at a predetermined level (3.5-20 cm H₂O), independent of whether or not oscillations were applied. Airway opening pressure (Pao) was measured through a lateral side arm at right angles to the 15 mm i.d. HFV delivery tube, using a rapidly responding pressure transducer (Ailtech MS-10); mean Pao was obtained by electronically low-pass filtering the pressure signal. Fifty or 100 ml sinusoidal oscillations (frequency 0.5-20 Hz) were provided by a sealed piston pump driven by a linear magnetic motor. Tidal volume was measured by integrating flow measured with a number 2 Fleisch pneumotachograph coupled with a Validyne MP-45 \pm 50 cm H₂O pressure transducer, calibrated as described previously (14) for each frequency-tidal volume combination to be employed.

The experimental protocol was as follows: End-tidal CO₂ fraction (Beckman LB-2) was maintained within 0.5% (4.8-5.3%) with a conventional tidal ventilator, using the patient's usual tidal volume at an appropriate frequency. The patient's tracheostomy tube was then disconnected from the conventional ventilator, and the patient was allowed to relax to functional residual capacity (FRC) (Pao=0) for 2-5 seconds, until lung volume (measured by the RespiTrace) was stable. The subject was then connected to the HFV apparatus (with the oscillator turned off), and allowed to reach a new stable lung volume determined by the prechosen mean Pao. Sinusoidal oscillations with prechosen frequency and tidal volume were then applied for 30-45 seconds. In this interval, CO₂ removal rate was measured as bias flow rate times mean bias flow CO₂ concentration (Beckman LB-2), and further changes in lung volume were measured by the impedance plethysmograph. The subject was then returned to the conventional ventilator (where FRC was shown to be statically determined), and the end-tidal CO₂ again measured. The entire sequence was repeated as HFV frequency and tidal volume and mean Pao were systematically varied.

B. Computational Model

A simple electrical circuit (Figure 2) was used to model the presumed mechanical behavior of the HFV pump, the bias flow, and the central and peripheral portions of the respiratory tree. In the analogy, current models volume flow, and voltage reflects pressure, with ground equal to atmospheric pressure. The HFV pump is thus a current source (I_{pump}); the bias flow is modeled with a voltage source (V_{map}), whose value represents mean airway pressure, coupled to the airway opening node by a large inductance (L_{bf}). This configuration results in a high impedance of the "bias flow" to oscillatory flow.

The respiratory tree has two parallel branches: a central airway "shunt" compliance (C_{aw}), which reflects potential radial oscillatory motion of the central airway walls, and an axial

path from the airway opening node to the alveolar node. Inspiratory and expiratory limbs of the latter path are isolated by ideal diodes to facilitate implementation of asymmetry; the inspiratory limb consists of a fixed inspiratory resistance (R_{insp}) leading to the alveolar capacitance (C_{alv}). To model each of three types of asymmetric airways impedance, we varied the structure of the expiratory limb: Fixed asymmetric resistance was modeled using a linear resistor (R_{exp}); variable asymmetric resistance was modeled with a variable resistance whose value varied inversely with lung volume [$R_{exp}(P_{alv} + 30 \text{ cm H}_2\text{O})$]; and expiratory flow limitation was modeled using an idealized PNP transistor to limit current at a value proportional to lung volume (P_{alv}), in series with a resistance equal to R_{insp} . In each case, P_{alv} equal to zero represents FRC; P_{alv} equal to $-30 \text{ cm H}_2\text{O}$ models residual volume. Component values were chosen to reflect relative physiologic of values.

Computer simulations of HFV were performed by an iterative integration computer program (SPICE2, copyright Univ. of Calif., Berkeley). Tidal volume was set to 100 ml; frequencies of 1-16 Hz were used. Mean airway pressures of 0, 5, and 10 $\text{cm H}_2\text{O}$ were studied for each type of asymmetry. Excursion extremes of P_{alv} and P_{ao} and mean P_{alv} were estimated from this simulation.

C. Gas Transport in Hardware Models

The objective of these tests was to determine the dispersion coefficient for transport during conditions simulating HFV in a hardware model. For this purpose, we set up a steady condition in which a trace gas is infused at a constant rate at the "alveolar" end of the network. Measurements are taken only after a quasi-steady state has been reached throughout the network. This state is achieved once the cycle-averaged concentration at each measurement location is steady, which, by conservation of mass, indicates that the cycle-averaged mass flow rate of tracer through each generation is uniform. This not only simulates the conditions of HFV under steady state conditions (O_2 and CO_2 being exchanged at constant rates) but also increases the accuracy of our experiments, since the measurement can be repeated over many oscillation cycles and averaged to eliminate extraneous noise.

The model used in the experiments consists of a system of rigid, constant diameter tubes, constructed from 1 cm nalgene "Y" connectors, as shown in Figure 5. Each bifurcation has a branching angle of 60 degrees and each tube segment has a length-to-diameter ratio of 3.5:1. Flow oscillations produced by 8 (16 in the four-generation experiments) synchronously driven pistons and a constant infusion of pure tracer gas were both introduced at the "alveolar" end of the model so as to eliminate any uncertainties concerning the distribution of flow to each branch. Studies (15) in a model geometrically similar to ours have indicated that the flow distribution among lateral and medial branches varies with flow rate and can be quite sensitive to small geometrical asymmetries.

The-tracer concentration was measured simultaneously at two sites using an infrared (IR) absorption technique. The attenuation of monochromatic radiation by a gas with absorptivity of β is given by Beer's law:

$$I = I_0 \exp(-\beta \bar{C} \Delta x) \quad (1)$$

where I is the attenuated intensity of radiation, I_0 is the unattenuated intensity, C is the average volume fraction of the absorbing gas along a beam path of length Δx . The experiments were conducted using a helium-neon laser operating at $3.391 \mu\text{m}$ (Jodon Model HN-5) and methane as the absorbing tracer gas because of the strong coincidence of the methane absorption band ($\beta = 9.4 \text{ cm}^{-1} \text{ atm}^{-1}$) and the laser wavelength.

The laser beam was chopped, then split into three beams. One beam was directed toward a PbSe IR detector while the other two were passed through glass coverslips mounted in the branching network at one pair of the locations identified in Figure 5.

At measurement location (i), the path length averaged concentration can be written as:

$$C = [k_i - \ln(e_i/e_r)]/2a\hat{\beta} \quad (2)$$

where e_r is the output voltage of the reference detector, a is the light path length, e_i is the output voltage of the optical detector at measurement location (i), and (k_i) is a constant which depends upon the alignment of the optical system.

We assume that the path length and cross-sectional averages are nearly equal to one another. This assumption breaks down in situations in which the cross-sectional variation in concentration is large. Even in these situations, however, we might expect the error at any two of the measurement locations identified in Figure 5 to be in the same direction, in which case the errors would tend to cancel when calculating the local concentration gradient.

The detector output signals were passed through an RMS-to-DC converter (eliminating the chopping frequency) and then digitally processed (using a DEC MINC-11 Data Acquisition System). Additional signals from a piston position transducer and phase indicator were also digitized and processed. The phase indicator initiates the data acquisition sequence causing the A/D converters to sequentially sample the input signals at a rate of 100 points per cycle over successive intervals 1.5 cycles long. This procedure was repeated from 20 to 100 times, and an ensemble average was computed to minimize random measurement error. The detector signals were then used to

compute instantaneous values of the tracer concentrations (equation [2]). The signal indicating piston position was used to compute the bulk oscillatory flow rate. Each of these signals, representing a time-varying profile over a 1.5 cycle period, was then stored in digital form.

Samples of typical concentration profiles at the various measurement locations are shown in Figure 6. The subscripts refer to measurement locations identified in Figure 5.

To conduct an experiment, the oscillatory flow and tracer infusion were started simultaneously, using a methane flow rate selected to achieve methane concentrations of 1-15% at the measurement sites. Concentrations were monitored until a steady state was reached in which the cycle-average concentrations no longer varied with time. At that point, measurements were simultaneously made at two locations. When the measurement was completed, the oscillations were stopped, the system was purged with fresh air and a reference measurement was taken corresponding to zero concentration.

Computer analysis of the signals from the IR detectors yields values of methane concentration as a function of time at the two measurement sites. In addition, the time-mean methane flow rate in each tube segment is known, since a steady state had been reached prior to measurement. Using measured values of the methane flow rate, q_m , values for an effective diffusivity can be computed from the following expression (see reference (16) for complete derivation).

$$D_{eff} = q_m (x_1 - x_2) \ln[(1 - C_1)/(1 - C_2)] \quad (3)$$

where subscripts "1" and "2" refer to two different measurement sites (either 1 and 2 or 2 and 3 in Figure 5). In writing this expression, we make the implicit assumption that the transport process is diffusive in character, as has been done by others in the past (8,17). However, neither our measurements nor those of others provide definitive evidence of the diffusive nature of the transport process. In fact, Haselton and Scherer (18,19) have demonstrated that the results of Scherer et al. (17) can be explained on the basis of a convective rather than diffusive process.

The values of D_{eff} determined from Equation (3) are fit, by a double least-squares method, to a correlation of the form:

$$D_{eff} - \chi = qV_t^r f^s \quad (4)$$

Here q , r , and s are coefficients determined experimentally, χ is the molecular diffusivity, V_t is the local tidal volume in the tube segment (i.e., total stroke volume divided by 2 for first generation and by 4 for second generation), and f is the

oscillation frequency. While other forms might be more appropriate, as, for example, that obtained by the theoretical analysis of Erdogan and Chatwin (20) for steady flow dispersion in curved tubes, the correlation obtained using Equation (4) provided a satisfactory fit of the data. This form is consistent with that used by Tarbell et al (8) to reduce their experimental results except that, for their experiments in liquid, it was not necessary to include the effects of axial molecular diffusion.

III. RESULTS

A. Experiments in Patients

The dependence of dynamic hyperinflation on frequency and on mean P_{ao} is illustrated in Figure 3. Using a 100 ml sinusoidal tidal volume, when mean P_{ao} was low ($2-5 \text{ cm H}_2\text{O}$), dynamic hyperinflation occurred at the lowest frequency applied (0.5 Hz) and increased with frequency so that a greater than 1 liter change in dynamic FRC was seen in two subjects. In contrast, when the mean airway pressure was raised ($7-13 \text{ cm H}_2\text{O}$), a different dependence of dynamic hyperinflation on frequency was observed. Although the elevated mean P_{ao} was itself associated with an elevated mean lung volume compared to resting FRC, there was no further increase in lung volume as frequency was raised, until the frequency reached some critical value (1.5-4 Hz). Above this critical frequency, lung volume did increase with frequency in a fashion parallel to that seen at the lower mean P_{ao} .

In contrast to the importance of mean alveolar pressure (MAP) in determining dynamic hyperinflation, changing MAP over a twofold range had little effect on the dependence of rate of CO_2 removal during HFV bursts on frequency. Figure 3 shows the curvilinear increase and plateau of \dot{V}_{CO_2} with frequency seen in these patients. These results are consistent with those found in prior investigations (4,13).

B. Predictions of Transistor Model

The dependence of MAP on frequency and mean P_{ao} predicted with each of the three asymmetric impedance models is illustrated in Figures 4a-4c. In each case, MAP is estimated as the mean of the oscillatory alveolar pressure extremes. When the expiratory limb of the respiratory path shows a fixed resistance whose magnitude is greater than that of the R_{insp} (Figure 4a), mean P_{ao} does not affect the dependence of mean P_{alv} on frequency at fixed tidal volume. In addition, for the higher mean P_{ao} 's, there is no range of frequencies in which mean P_{alv} is independent of frequency at fixed tidal volume. Predictions obtained using a variable R_{exp} which varies inversely with lung volume (Figure 4b) are generally similar, though the rate of increase of mean P_{alv} with frequency becomes slightly smaller as mean P_{alv} increases, reflecting the progressive diminution of asymmetry of inspiratory and expiratory resistances. Thus, predictions of both the fixed and

variable Rexp models are qualitatively different from the dependence of mean lung volume (and presumably mean Palv) on HFV frequency and MAP observed in our patients. In contrast, the dependence of mean Palv on frequency and Map predicted in the expiratory flow limitation model (Figure 4c) does qualitatively resemble that observed in our patients (Figure 2).

C. Gas Transport Model Experiments

The purpose of these experiments was to study and quantify gas transport during HFV. The range of experimental parameters was therefore selected to overlap, as much as possible, the range of HFV conditions found previously (4) to maintain adequate gas exchange in human subjects. In dimensionless terms, the experiments span a range of Peclet number ($Pe=2Ua/\kappa$ where U is the cross-sectional mean velocity amplitude, a is the vessel radius, and μ is the molecular diffusivity) from 5-1100 and dimensionless frequency $\beta = \alpha (\omega/\kappa)^{1/2}$ where ω is the angular frequency from 1-12. In dimensionless terms, this range of Pec and B corresponds to tidal volumes ranging from 2-40 cc and frequencies from 0.2-13 Hz. At a tidal volume of 50 cc and a frequency of 15 Hz, this corresponds to generations 5-13 in a lung with the morphology given by Weibel (12). These results cannot be directly applied to the first several generations both because of this constraint on Pe and also because the turbulence generated by a tracheal catheter or glottal aperture is absent in our tests.

In the calculation of D_{eff} using Equation (3), the time-averaged concentration is used. Our measurement technique, however, had sufficient time resolution to discern time variations in concentration during the course of an oscillation cycle. Two typical traces of concentration versus time are shown in Figure 6.

Two series of experiments were conducted that span roughly the same range of parameters. In the first (series A), measurements were made across the first generation of the branching tree, at positions 1 and 2 (see Figure 5). In the second (series B), concentrations were measured across the second generation at 2 and 3. Since we anticipated differences in the two data sets, we performed the curve-fitting analysis on each set separately. In addition, we found that the results from series A satisfied different relations depending on the range of dimensionless frequency. The correlations of all our data are presented in Table 2, including the single expression obtained when all the data from both generations were analyzed together.

Shown also in Table 2 are values for a second set of constants corresponding to the dimensionless relationship (see dimensional analysis below):

$$\mathcal{D} = (D_{eff} - \tau) / \kappa = \tilde{q} Pe \tilde{r} \beta^{\tilde{s}} \quad (5)$$

While it is convenient to express our results in dimensionless form, the dependence on molecular diffusivity suggested by this equation has not been tested in our experiments, since we used a single gas mixture. Consequently, the dimensionless transport coefficient given above may also exhibit a dependence on Schmidt number not evident in our experiments.

The fit of our data to this particular form can be seen by plotting $(D_{eff}/\kappa - 1)/(q \bar{c}^2)$ vs. Pe . According to Equation (5), this plot has a slope of r on a log-log plot as shown in Figure 7.

IV. DISCUSSION

A. Patient Experiments

The data we report here confirm and extend previous observations (1,2). In our patients, the rate of alveolar ventilation during HFV with either 50 or 100 ml tidal volumes increased with frequency until a critical frequency was reached; above this frequency, no further increase in \dot{V}_{CO_2} (reflecting alveolar ventilation) was found with increases in oscillatory frequency. In addition, there was little change of \dot{V}_{CO_2} with mean Pao over the approximately twofold range studied. Each of these results coincides with previous observations on HFV-mediated gas exchange (4,14). Our findings of asymmetric Pao fluctuations around the mean and of impressive dynamic pulmonary hyperinflation also confirm previous reports in humans (2) and in animals (1).

Two features of our data represent new observations. First, while alveolar ventilation appears to depend on oscillatory frequency, dynamic hyperinflation is more directly related to expiratory flow. In the two patients in whom tidal volumes of 50 and 100 ml were applied using similar mean Pao 's the plateau of \dot{V}_{CO_2} occurred at about the same frequency for either tidal volume. However, the frequency at which equal degrees of dynamic hyperinflation occurred was about twice as large when the smaller tidal volume was used than when the larger tidal volume was applied. This finding indicates that it is flow, rather than frequency, which determines dynamic hyperinflation at a given mean Pao . Although previous investigations (2) suggested this result, the simultaneous \dot{V}_{CO_2} and lung volume measurements reported here strengthen this conclusion. In addition, our finding that at the same oscillatory frequency and tidal volume and similar mean airway pressure, shorter expiratory times markedly enhance lung hyperinflation further suggests that it is expiratory flow, rather than average or inspiratory flow, which is related most closely to this phenomenon.

Second, in contrast to its minor influence on alveolar ventilation, mean Pao is an important determinant of the relationship between dynamic hyperinflation and oscillatory flow (Figure 3). When mean Pao was higher, there was, of course, static elevation of lung volume above the resting FRC. However, further dynamic hyperinflation did not occur at many flow rates that did increase lung volume above the lower static lung volumes associated with lower mean Pao's. This finding suggests that if asymmetry of inspiratory and expiratory impedances accounts for dynamic hyperinflation, then the asymmetry first appears with increasing flow at relatively lower flow rates when the lung volume is lower, and at rather higher flow rates when the lung volume is higher. Maximal expiratory flow limitation behaves in this manner. These two new observations suggest that maximal expiratory flow limitation occurs during HFV, and substantially accounts for dynamic pulmonary hyperinflation.

To examine other potential mechanisms of asymmetric oscillatory impedance during HFV, we applied the simple electrical analog of mechanical events during HFV illustrated in Figure 2. We considered three forms of asymmetry which might be extant: fixed asymmetric resistance, variable asymmetric resistance, and expiratory flow limitation with equal inspiratory and expiratory resistances. By examining predictions from these models, it is clear that only expiratory flow limitation results in a dependence of dynamic hyperinflation on oscillatory flow and mean airway opening pressure (assuming that mean alveolar pressure reflects lung volume [Figure 4]) which resembles that found in our patients. It is of particular note, though, that the other feature which suggests asymmetry of inspiratory and expiratory impedances, namely, asymmetric fluctuations about the mean airway opening pressure, is qualitatively similar among the three models, at least for the higher flow rates at which dynamic hyperinflation occurs. Therefore, this finding of asymmetric airway opening pressure excursions alone does not allow us to distinguish among the mechanisms potentially responsible for dynamic hyperinflation.

Another feature similar among the three models is the predicted distribution of flow introduced into the trachea (airway opening node). In each case, for a given tracheal tidal volume, the central airway wall motion "shunt" volume increases with frequency and varies only little with mean airway opening pressure. Conversely, the peripherally delivered tidal volume ($V_{T_{alv}}$) falls with frequency above the critical frequency; thus, peripherally delivered flow (frequency times $V_{T_{alv}}$) rises with frequency until it starts to plateau at the critical frequency. Like central airway "shunt" volume, peripheral flow depends little on mean airway opening pressure. The similarity in these dependences of predicted peripheral flow and of observed \dot{V}_{CO_2} on HFV frequency and mean airway opening pressure at constant tracheal tidal volume is striking, but does not necessarily imply a causal relationship. Nonetheless, that each of the three asymmetric impedance models predicts similar dependences of peripheral flow on frequency and MAP means that this behavior

does not-discriminate among these potential modes of asymmetry.

Our data clearly indicate that flow limitation is most likely responsible for dynamic hyperinflation during HFV; what is still not established is the relationship of this limitation to gas transport during HFV. To gain better understanding of the latter problem, we studied gas transport in hardware models.

B. Hardware Model Studies

1. Effects of Model Geometry

One objective of these experiments was to determine expressions that can be used in model simulations of gas exchange during typical conditions of HFV. The extent to which these results are useful for this purpose depends upon the realism incorporated into the model. In our experiments several geometrical features of the model differ from those typically found in the lung. For example, the transition from one generation to the next is abrupt in the model in that the corners are sharp and the change in area (a factor of two at each branch) is larger than one typically finds in the airways. These differences are likely to promote flow separation, especially during inspiration. The velocity fluctuations and eddy motion associated with the separated region could influence the rate of gas exchange. The same factors could cause an earlier transition to turbulence in the model than in the lung, but since the peak values of Stokes layer Reynolds number (Re/α dimensionless frequency) in our tests were always less than 200, it seems unlikely that we entered the turbulent regime (2). Furthermore, we found no evidence in our experimental results to suggest a transition to turbulence as observed by Azhar and Tarbell (9).

2. Boundary Effects

In experiments conducted in networks with relatively few generations, one must also consider the importance of end effects. We would expect, for example, that fluid near the ends would exhibit less mixing due to secondary flow, since that fluid resides in a straight tube segment during a larger part of the cycle than fluid in the more central regions of the model. This effect would be most evident in measurements made at the first generation, where the mean fluid displacement is greatest. We found, however, that the differences between the first and second generations (series A and B) were relatively small. Although the curve-fitting procedure yields somewhat different results for the two test series (Table 2), when the two data sets are combined, there is a relatively small decrease in the accuracy of the curve fit.

In analyzing the data, we obtained the best fit to the data by dividing the results from series A into two groups, depending on whether α was $>$ or $<$ 4. However, we found no clear advantage when the series B results were processed in the same way. While

this seems to suggest that the transition to quasi-steady flow occurs at lower values of β , this may simply reflect the relatively large experimental error in these low frequency measurements as well as the narrow range of β tested. To resolve these questions will require more extensive tests at yet lower values of β .

3. Dimensional Analyses of Unsteady Dispersion

To provide a framework for the consideration of the effects of unsteadiness and molecular diffusion to follow, we first cast the axial dispersion coefficient in non-dimensional form. In dimensional terms, we express $(D_{eff}^{-\kappa})$ (representing transport above and beyond that due to axial diffusion alone) as a function of six dimensional parameters:

$$D_{eff} = f_1(U, a, T, \nu, \kappa, g) \quad (6)$$

where T is the period of oscillation ($T = 2\pi/\omega$), and g symbolically represents all the parameters associated with airway geometry. A dimensionless form of (6) is:

$$(D_{eff}^{-\kappa})/U^2T = f_2(Pe, \beta, Sc, G) \quad (7)$$

where Sc is the Schmidt number ($Sc = \nu/\kappa$) and G denotes all dimensionless parameters having to do exclusively with system geometry.

The dimensionless time in this expression is the square of the ratio formed by the radial diffusion time ($\tau_{rad} = a^2/\kappa$) and the cycle period (T). Therefore we can rewrite (7) as:

$$(D_{eff}^{-\kappa})/U^2T = f_n(Pe, \tau_{rad}/T, Sc, G) \quad (8)$$

When the theoretical results for laminar oscillatory flow dispersion in a straight tube (22) are expressed in the form of Equation (8), we obtain the curve plotted in Figure 8. The comparison in Figure 8 provides information on the importance of G in Equation (8). Note that when τ_{rad} alone is decreased, the rate of dispersion will either decrease or increase, depending on whether τ_{rad} is $<$ or $>$ T , respectively.

An alternate but entirely equivalent dimensionless form can be derived which is useful in comparing our results to those of other investigators.

$$\mathcal{D} = (D_{eff}^{-\kappa})/\kappa = f_n(Pe, \beta, Sc, G) \quad (9)$$

Under certain circumstances, one or more of the dimensionless groups in Equation (9) can be eliminated. Several examples are of particular interest in the following discussions: (1) If the flow were quasi-steady, then D would be independent of β . (2) If the flow were highly turbulent, convective mixing would overwhelm the effects of molecular diffusion, Sc would consequently have little effect and α should be replaced by ν . (3) If the flow were both quasi-steady and highly turbulent, we would expect D to be independent of both β and Sc .

4. Comparison to Other Experiments.

Because of substantial differences between our experiments and those of Tarbell et al. (8) and Scherer et al. (17) (hereafter referred to as Tarbell and Scherer), direct comparisons are difficult. The major difference is that while our measurements are local in the sense that we determine D_{eff} from the concentration gradient across a single generation, both Tarbell and Scherer measured the rate of dispersion over the entire branching network, and their results are therefore influenced to varying degrees by the local transport process in each individual generation.

Despite these differences, some useful comparisons can be made. In order to cast all the results in comparable form, we first note that the dispersion expressions obtained by Tarbell and Scherer represent a network average. We will assume that the dependence they observe on Reynolds or Peclet number (and α for Tarbell) is consistent throughout all generations. Accordingly, the rate of dispersion is greatest in the lower generations, where the highest Reynolds numbers are encountered. The network dispersion coefficient that they define, therefore, can be thought of as a weighted average of the local values of D_{eff} . When casting their results in dimensionless form, Tarbell uses the total cross-sectional area of the second generation as the approximate "network area." In the following comparison, we assume that the network dispersion coefficients defined by Scherer and Tarbell are roughly equivalent to the dispersion coefficient in their second generations. While this is somewhat arbitrary, the error in the approximation is likely to be relatively small and will affect only the numerical constant (e.g., q and q in Equation [5]) and not the exponents. Based on these assumptions, we will express the results of Scherer and Tarbell in terms of the Peclet number in the second generation (based on tube diameter). We relate Tarbell's Reynolds number ($Re_T = U_0 a / \nu$ where U_0 is the velocity amplitude in the parent tube of the network) to a local one, using:

$$Re = Re_T / 2$$

Dimensionless dispersion coefficients are thus obtained for the results of Tarbell:

$$D_T = 0.0035 Sc (Pe Sc)^{1.82} a^{-0.86} \quad (10)$$

and Scherer:

$$D_S = 0.9 Pe \quad (11)$$

While we have introduced Sc to Equation (10) to be consistent with Tarbell's dimensionless formula, in the following comparisons Sc is set equal to unity.

Within the range of Reynolds number and dimensionless frequency investigated in both unsteady experiments (which also overlap the range of Peclet number tested by Scherer), the comparison of Figure 9 can be made for a gas mixture with $Sc = 1$. Note that in placing Tarbell's correlations on this graph, we have implicitly assumed that mixing by molecular diffusion is unimportant and, therefore, that Tarbell's results are unaffected by Schmidt number. The validity of this assumption is considered later.

More recently, Azhar and Tarbell (9), using methods similar to those of Tarbell, have shown that their network dispersion coefficient D_N takes on one of two forms:

$$D_N \propto Re^{1.43} a^{-1.64} \quad (12)$$

for low Re , and:

$$D_N \propto Re^{1.57} \quad (13)$$

for high Re . They found that the transition value of Re depended on oscillation volume and ranged from 2,000 to 9,500 in their experiments.

5. The Effect of Unsteadiness

As noted earlier, the transport process is quasi-steady when $\tau_{rad}/T > 1$, leading to a result in which D_{eff} is found to be independent of τ_{rad}/T . Our expressions for D_{eff} show a clearly significant dependence upon τ_{rad}/T (or τ_{rad}/T), at least for values of $\tau_{rad}/T > 4$ (see Table 2), suggesting that generally $\tau_{rad}/T < 1$. The data for $\tau_{rad}/T < 4$ are inconclusive in this regard, largely because of a limited amount of data in this range. By

comparison, the results of Tarbell given in Equation (11) yield a smaller, yet non-zero exponent for β .

However, the more recent data from Azhar and Tarbell show two distinct regimes depending on whether Re is above or below some transition value. Their high Re correlation is independent of α and therefore quasi-steady. The reason for this, presumably, is that turbulent mixing decreases the radial equilibration time so that τ_{rad}/T becomes < 1 . The low Re correlation from Azhar and Tarbell bears a striking resemblance to ours (Table 2) in terms of the exponents on Re and α . In both cases the result appears to be intrinsically unsteady.

We can also compare our low frequency results to those of Scherer et al. (1975) for steady flow through a branching network. Taking all our data from both generations for $S < 4$, we find that the ratio D/D_S has a mean value of 0.50 with a standard deviation of 0.30 for the 24 experimental points within this range of β . It has been suggested by Pedley (22) that a more appropriate unsteadiness parameter in a branching network is $\epsilon = \omega L/U$ (where L is the generation length). Choosing those data for which $\epsilon < 1$ (37 data points), the mean value for D/D_S is 0.62 ± 0.22 . Thus both the approximate agreement in form between Scherer's findings and our low frequency results and the good numerical agreement indicated by the values for D/D_S given above support our claim that these low frequency experiments are quasi-steady.

6. The Effect of Molecular Diffusion

Based on the comparison in Figure 9, there appears to be reasonably close agreement between our results and those of Tarbell in view of the approximations on which the comparison is based. Even closer correspondence is found between our data and the low Re data of Azhar and Tarbell. All this suggests that molecular diffusion plays at most a small role in the transport process of these experiments. This conclusion is consistent with the results of Knopp et al. (23), who found no significant effect of molecular diffusivity in the rate of tracer clearance from dog lungs during high frequency oscillation.

There is reason to believe, however, that some differences might exist between liquids and gases, based on experimental results of dispersion under steady flow conditions, even when the flow is turbulent or in the presence of secondary flow. In a comparison between the theoretical prediction of Taylor (24) for axial dispersion under conditions of steady flow in a straight tube and experimental results, Levenspiel (25) has attributed the observed differences to the effects of molecular diffusion. Gas and liquid experiments conducted in curved tubes with secondary flows also exhibit large differences in axial dispersion in the range $Re < 10^4$ (van An del et al, 26). Thus, while the results obtained in branching tubes are not, by themselves, sufficient to show a significant effect of Sc , experiments in other configurations suggest that some differences may exist between liquids and gases.

7. Conclusion

Correlations have been present that are applicable to models of HFV in the lung. These demonstrate that tidal volume exerts a greater influence than frequency of oscillation, consistent with the measurements of gas exchange during HFV in test animals.

Our results show a significant dependence on dimensionless frequency, demonstrating that, at least for Reynolds numbers up to about 1000 and values of $\beta > 4$, the effects of unsteadiness are important. Our data lie remarkably close to the results for oscillatory flow in a straight tube but are higher. This enhancement of axial transport can be attributed to one or more of the following mechanisms: increased cross-stream mixing, a less uniform axial velocity profile (both of which enhance augmented dispersion), and convective streaming.

There remain, however, a number of uncertainties. Among these are questions pertaining to the importance of molecular diffusion at both low and high Reynolds numbers and the effect of and conditions for a transition from laminar to turbulent flow. In addition, the relative importance of streaming versus augmented dispersion in all the experiments conducted in branching networks needs to be examined further.

V. MILITARY SIGNIFICANCE

Ventilatory assist by HFV may be used in battlefield resuscitation of chemical casualties. Our studies have provided basic information about gas trapping and gas transport in this circumstance. This could be of great value in the design of practical portable ventilators.

REFERENCES

1. Simon, B., Weinmann, G., and Mitzner, W.: Significance of mean airway pressure during high frequency ventilation (HFV). *Physiologist*. 25: 282, 1982.
2. Saari, A.F., Rossing, T.H., Solway, J., and Drazen, J.M.: Lung Inflation during High-Frequency Ventilation. *Am Rev. Respir. Dis.* 129: 333-336, 1984.
3. Gavriely, N., Solway, J., Loring, S.H., Ingram, R.H., Jr., Brown, R., Slutsky, A.S., and Drazen, J.M.: Airway dynamics during high frequency ventilation (HFV): a cineradiographic study. *J. Appl. Physiol.* 58: 645-652, 1985.
4. Rossing, T.H., Slutsky, A.S., Lehr, J., Drinker, P., Kamm, R.D., and Drazen, J.M.: Tidal volume and frequency dependence of carbon dioxide elimination by high frequency ventilation. *N. Eng. J. Med.* 305: 1375-1397, 1981.
5. Fredberg, J.J.: Augmented diffusion in the airways can support pulmonary gas exchange. *J. Appl. Physiol: Respirat. Environ. Exercise Physiol.* 49: 232-238, 1980.
6. Slutsky, A.S., Drazen, J.M., Ingram, R.H., Jr., Kamm, R.D., Shapiro, A.H., Fredberg, J.J., Loring, S.H. and Lehr, J.: Effective pulmonary ventilation with small volume oscillations at high frequency. *Science*. 209: 609-611, 1980.
7. Kamm, R.D., Drazen, J.M., and Slutsky, A.S.: High frequency ventilation. *Critical Reviews in Bioengineering*. 94: 347-349, 1984.
8. Tarbell, J.M., Ultman, J.S., and Durlofsky, L.: Oscillatory dispersion in a branching tube network. *J. Biomech. Engineering*, 104: 338-342, 1982.
9. Azhar, N., and Tarbell, J.M.: Axial dispersion during oscillatory flow in a lung model. *Proc. 36th ACEMB*, 1983.
10. Ultman, J.S., Tarbell, J.M., and Glickstein, S.: Oxygen mixing in lung airway models - Frequency effects. *Proc. 35th ACEMB*, 26, 1982.
11. Kamm, R.D., Collins, J.M., Joshi, C.H., Greiner, M., and Shapiro, A.H.: Axial dispersion of a passive contaminant in oscillatory flow. *Proc. 35th ACEMB*, 23, 1982.
12. Weibel, E.: *Morphometry of the human lung*. New York: Academic Press (Springer-Verlag), 1963.
13. Rossing, T.H., Solway, J., Saari, A.F., Gavriely, N., Slutsky, A.S., Lehr, J.L., and Drazen, J.M.: Influence of the Endotracheal Tube on CO₂ Transport during High-Frequency Ventilation. *Am. Rev. Respir. Dis.* 57: 54-57, 1984.

14. Slutsky, A.S., Kamm, R.D., Rossing, T.H., Loring, S.H., Lehr, J., Shapiro, A.H., Ingram, R.H., Jr., and Drazen, J.M.: Effects of frequency, tidal volume and lung volume on CO₂ elimination in dogs by high frequency (2-30 Hz), low tidal volume ventilation. *J. Clin. Invest.* 68: 1475-1484, 1981.
15. Snyder, B., Dantzker, D.R., and Jaeger, M.J.: Flow partitioning in symmetric cascades of branches. *J. Appl. Physiol.: Respirat. Environ. Exercise Physiol.* 51: 598-606, 1981.
16. Joshi, C.H., Kamm, R.D., Drazen, J.M., and Slutsky, A.S.: Gas exchange in laminar oscillatory flow. *J. Fluid Mech.* 133: 245-254, 1983.
17. Scherer, P.W., Schendalman, L.H., Greene, N.M., and Bouhuys, A.: Measurement of axial diffusivities in a model of the bronchial airways. *J. App. Physiol.* 38: 719-723, 1975.
18. Haselton, F.R. and Scherer, P.W.: Convective mixing in tube networks. *AICHE J.* 25: 542, 1979.
19. Haselton, F.R., and Scherer, P.W.: Flow visualization of steady streaming in oscillatory flow through a bifurcating tube. *J. Fluid Mech.* 123: 315-333, 1982.
20. Erdogan, M.D., and Chatwin, P.C.: The effects of curvature and buoyancy on the laminar dispersion of solute in a horizontal tube. *J. Fluid Mech.* 29: 465-484, 1967.
21. Akhavan, R.: Pressure-flow characteristics of a branching network during oscillatory flow. S.M. thesis, MIT, 1982.
22. Pedley, T.J., Schroter, R.C., and Sudlow, M.F.: Gas flow and mixing in airways. In: *Bioengineering Aspects of the Lung*, edited by J.B. West. New York: Marcel Dekker, 1977.
23. Knopp, T.J., Kaethner, T., Meyer, M., Render, R., and Scheid, P.: Gas mixing in the airways of dog lungs during high-frequency ventilation. *J. Appl. Phys.: Respirat. Environ. Exercise Physiol.* 55: 1141-1146, 1983.
24. Taylor, G.I.: The dispersion of matter in turbulent flow through a pipe. *Proc. R. Soc. Lond. (Biol.)* A 223: 446, 1954.
25. Levenspiel, O.: Longitudinal mixing in fluids flowing in circular pipes. *Ind. Eng. Chem.* 50: 343-346, 1958.
26. van An del, E., Kramers, H., and de Voogd, A.: The residence time distribution of laminar flow in curved tubes. *Chem. Eng. Science* 19: 77-79, 1964.
27. Watson, E.J.: Diffusion in oscillatory pipe flow. *J. Fluid Mech.* 133:245-254, 1983.

GLOSSARY

English

a	= Distance along a path
c	= Volume fraction of absorbing gas
Calv	= Alveolar compliance
Caw	= Central airway shunt compliance
cm	= Centimeter
Deff	= Effective diffusivity
Dn	= Network dispersion coefficient
Ds	= Diffusion coefficients given by Scherer (17)
Dt	= Diffusion coefficients given by Tarbell (8)
ei	= Output voltage of detector - experimental
er	= Output voltage of detector - reference
f	= Frequency
FRC	= Functional residual capacity
G	= Geometric coefficients
HFV	= High frequency ventilation
Hz	= Hertz (cycles per second)
I	= Laser intensity - experimental
Ibf	= Bias flow inductance
Io	= Laser intensity - reference
I _{pump}	= Current source for HFV
Ki	= Optical system constant
ln	= Natural logarithm
MAP	= Mean airway pressure
Palv	= Alveolar pressure
Pao	= Airway opening pressure
Pe	= Peclet Number
Re	= Reynolds Number
R _{exp}	= Expiratory resistance
R _{insp}	= Inspiratory resistance
Sc	= Schmidt Number
T	= Oscillation period
\bar{u}	= Velocity (mean)
\dot{V}_{CO_2}	= Rate of CO ₂ removal by HFV
V _{map}	= Mean airway opening voltage
Vt	= Tidal volume

Glossary (Continued)

Greek

- λ = Molecular diffusivity
 ϵ = Gas absorbtivity
 q = Regression constant
 r = Regression constant
 s = Regression constant
 \tilde{q} = Regression constant
 \tilde{r} = Regression constant
 \tilde{s} = Regression constant
 β = Dimensionless frequency based on molecular diffusivity
 α = Dimensionless frequency based on gas viscosity
 ω = Angular frequency
 τ_{rad} = Radial diffusion time
 σ = Unsteadiness parameter ($\omega \times \text{length}/V$)
 ν = Kinematic Viscosity

Figure 1

CO₂ removal rate (\dot{V}_{CO_2}) versus oscillatory frequency during short bursts of high frequency oscillation at fixed tidal volume, from each of three patients. Triangles connected by solid lines present data gathered with low mean airway pressure (~ 3 cm H₂O); squares connected by broken lines present data gathered with high mean airway pressure (~ 10 cm H₂O). \dot{V}_{CO_2} increases with oscillatory frequency up to a critical frequency (1-2 Hz), above which there is no further increase in \dot{V}_{CO_2} . There is no consistent dependence of the pattern of \dot{V}_{CO_2} versus frequency on mean airway pressure.

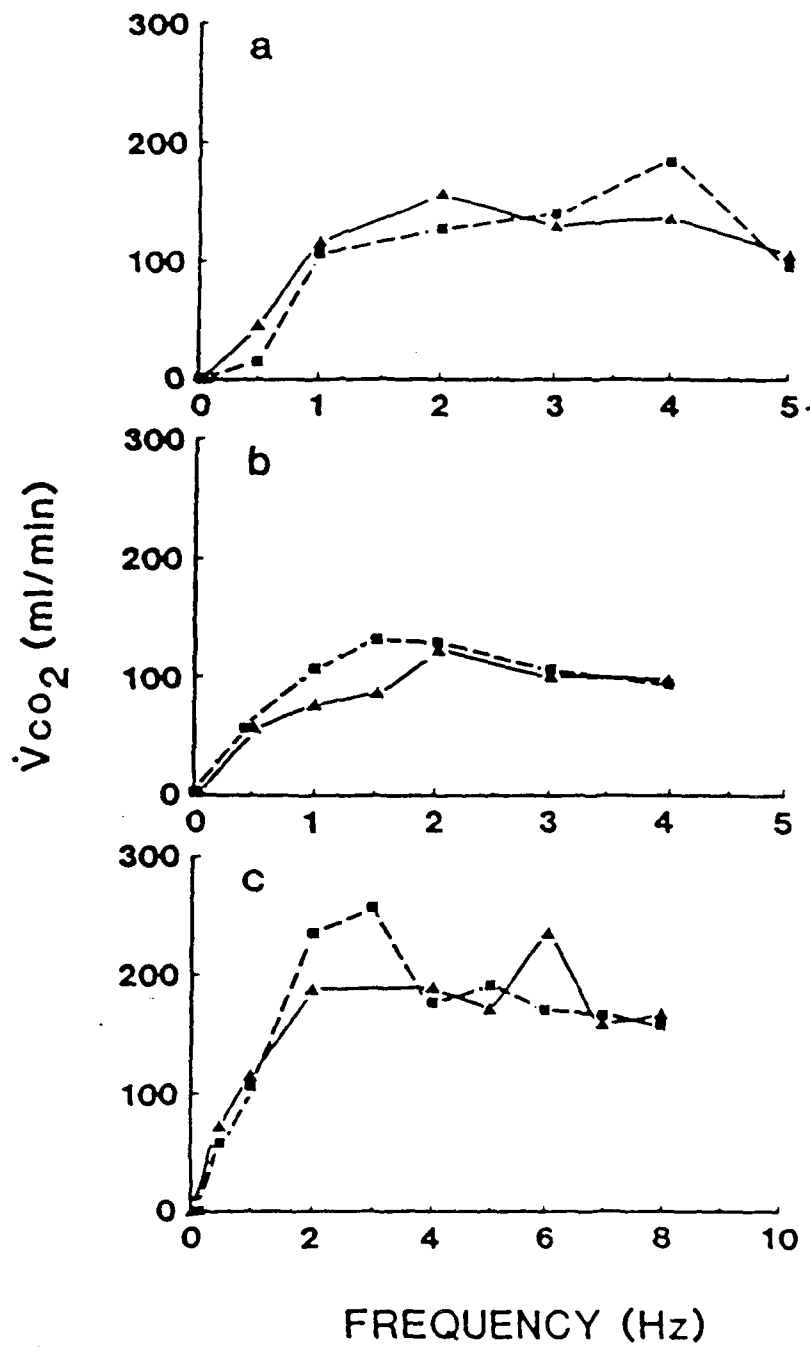
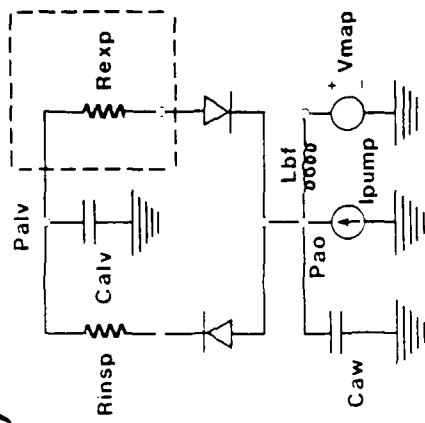


FIGURE 1

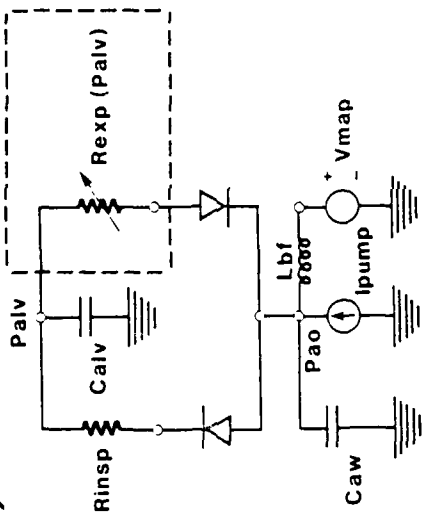
Figure 2

Three models of the mechanical events potentially responsible for dynamic hyperinflation during HFV. In each, the mean airway opening pressure is maintained by a pressure source (V_{map}) connected to the airway opening node by an inertance, which allows steady pressure to be transmitted while excluding oscillations from entering V_{map} . The oscillations are provided by a current source (I_{pump}), and may enter either a shunt compliance provided by the central airways (C_{aw}) or may proceed further in the axial direction toward the alveoli (whose compliance is C_{rs}). Within this axial path, inspiratory flow is separated from expiratory flow by idealized diodes. In each inspiratory path, the inspiratory resistance is identical (R_{insp}). The three models differ only in the expiratory limb of the axial path (enclosed within dashed lines). Model (a) includes a fixed expiratory resistance (R_{exp}), which is 5 times larger than R_{insp} . Model (b) includes a variable expiratory resistance [$R_{exp}(P_{alv})$], which decreases as lung volume is increased; its value is 5 times that of R_{insp} when $P_{alv} = +30$ cm H_2O total lung capacity [TLC] and 10 times R_{insp} when $P_{alv} = 0$ cm H_2O (FRC). Model (c) includes an expiratory resistance equal to R_{insp} , but also contains a transistor which models flow limitation so that the maximum possible flow through the expiratory limb increases linearly as lung volume (reflected in P_{alv}) increases. Values of V_{crit} and the flow limiting resistor were chosen so that V_{max} at FRC is 1.26 liter/sec and V_{max} at TLC is 2.51 liter/sec. Predictions of these models are shown in Figure 4.

a)



b)



c)

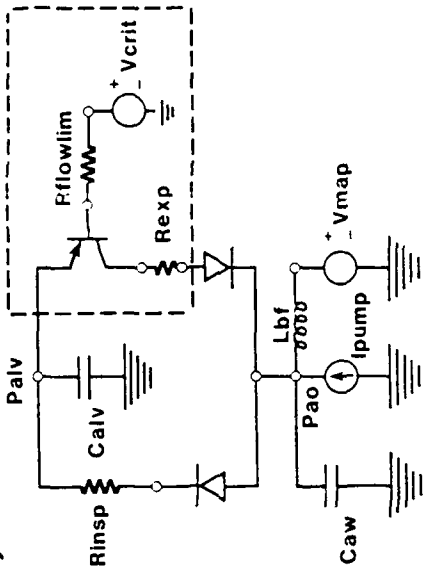


Figure 3

Elevation of lung volume above resting FRC during HFV as a function of oscillation frequency, with fixed tidal volume. With low mean airway pressure (~ 3 cm H_2O) (triangles and solid lines), there is a steady increase in dynamic hyperinflation with frequency. With high mean airway pressure (~ 10 cm H_2O ; squares and broken lines), the pattern differs: Although the high mean airway pressure has itself increased lung volume, no further increase occurs with frequency until a critical frequency (2-5 Hz) is reached. As oscillatory frequency is increased further, dynamic hyperinflation occurs, in a manner parallel to that seen with low mean airway opening pressure. Note that the critical frequency for dynamic hyperinflation at high mean airway opening pressure is not the same as the frequency at which \dot{V}_{CO_2} plateaus (see Figure 1).

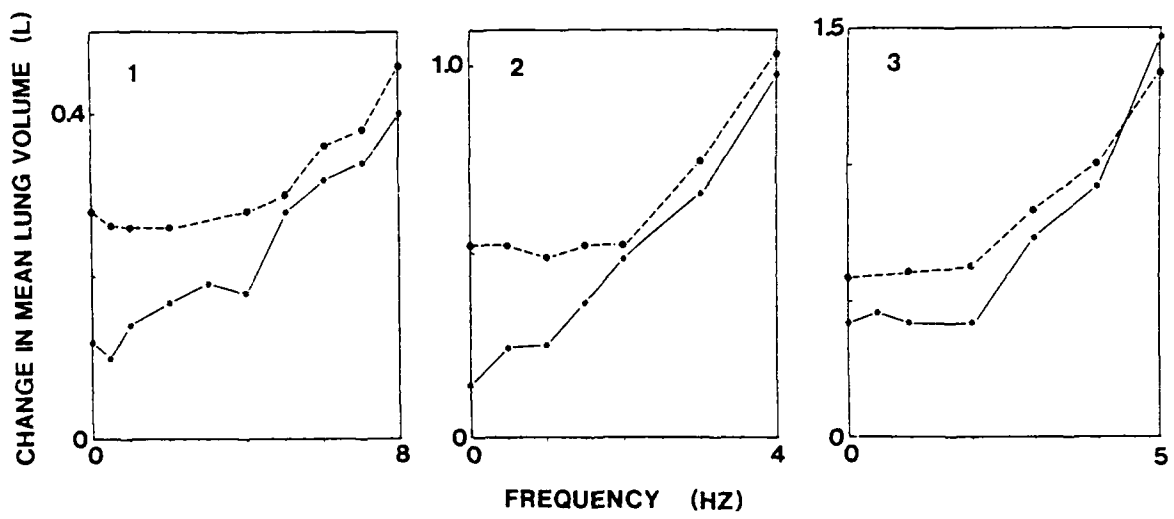


Figure 4

Predicted dynamic hyperinflation (manifest as increased P_{alv} above 0 cm H_2O [resting FRC]) versus frequency at fixed tidal volume (100 ml) for each of the three models shown in Figure 3. Both models (a) and (b) display progressive dynamic hyperinflation with increasing oscillatory frequency at either low mean airway pressure (0 cm H_2O ; squares and dashed lines) or high mean airway pressure (10 cm H_2O ; triangles and solid lines). Only model (c), which incorporates expiratory flow limitation, displays the plateau of lung volume over the low frequency range with high mean airway pressure, and the similar dynamic hyperinflation above a critical frequency, that were seen in our patients (see Figure 3).

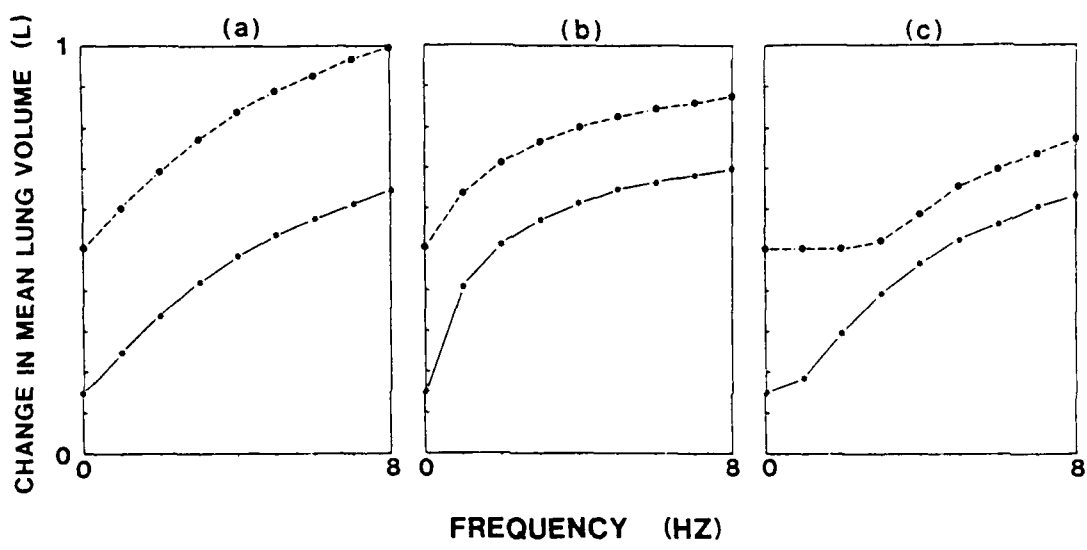


Figure 5

Branching network used in the experiments. Shown is the three-generation network. The four-generation network contains one additional generation with 16 pistons.

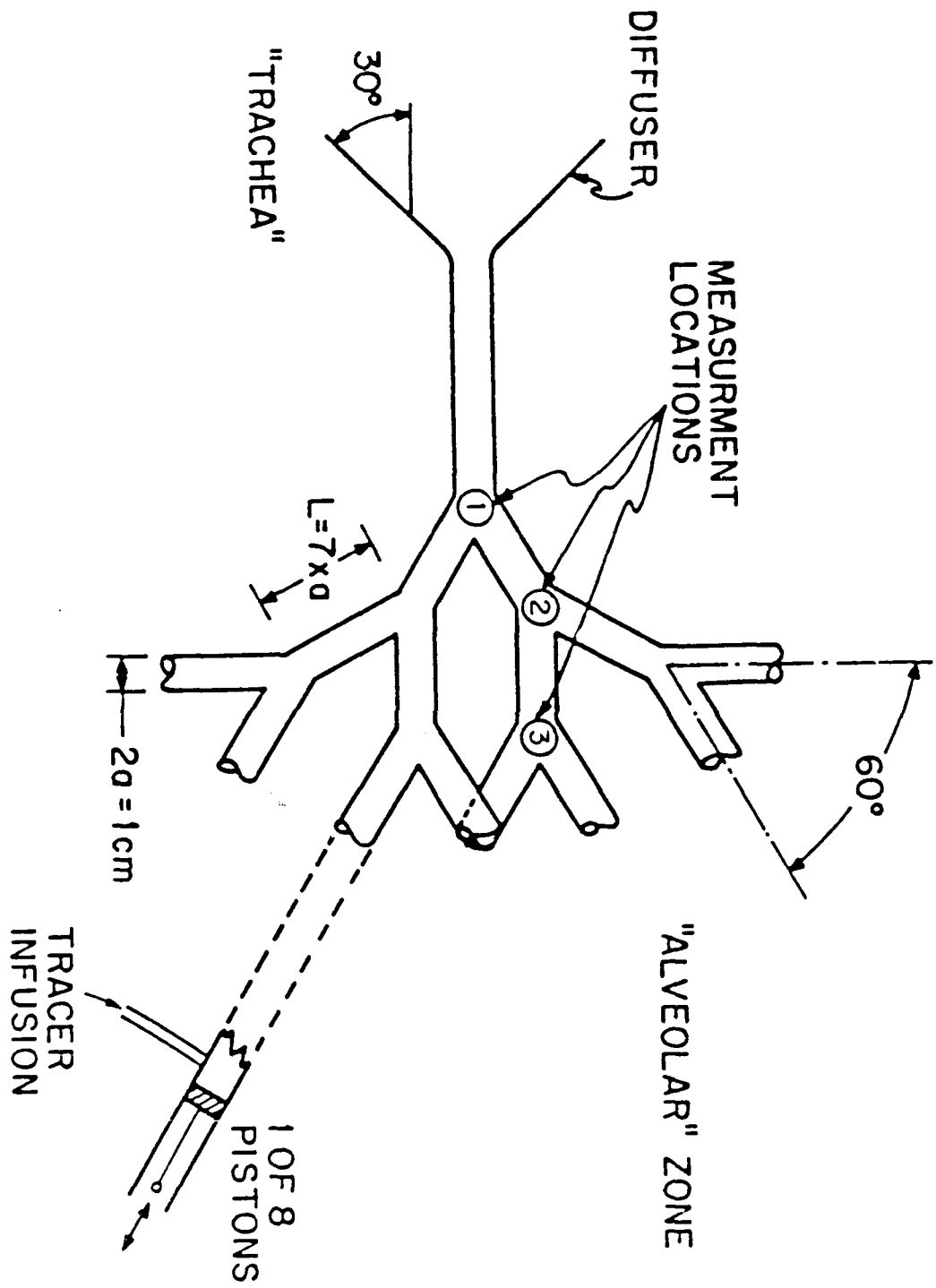
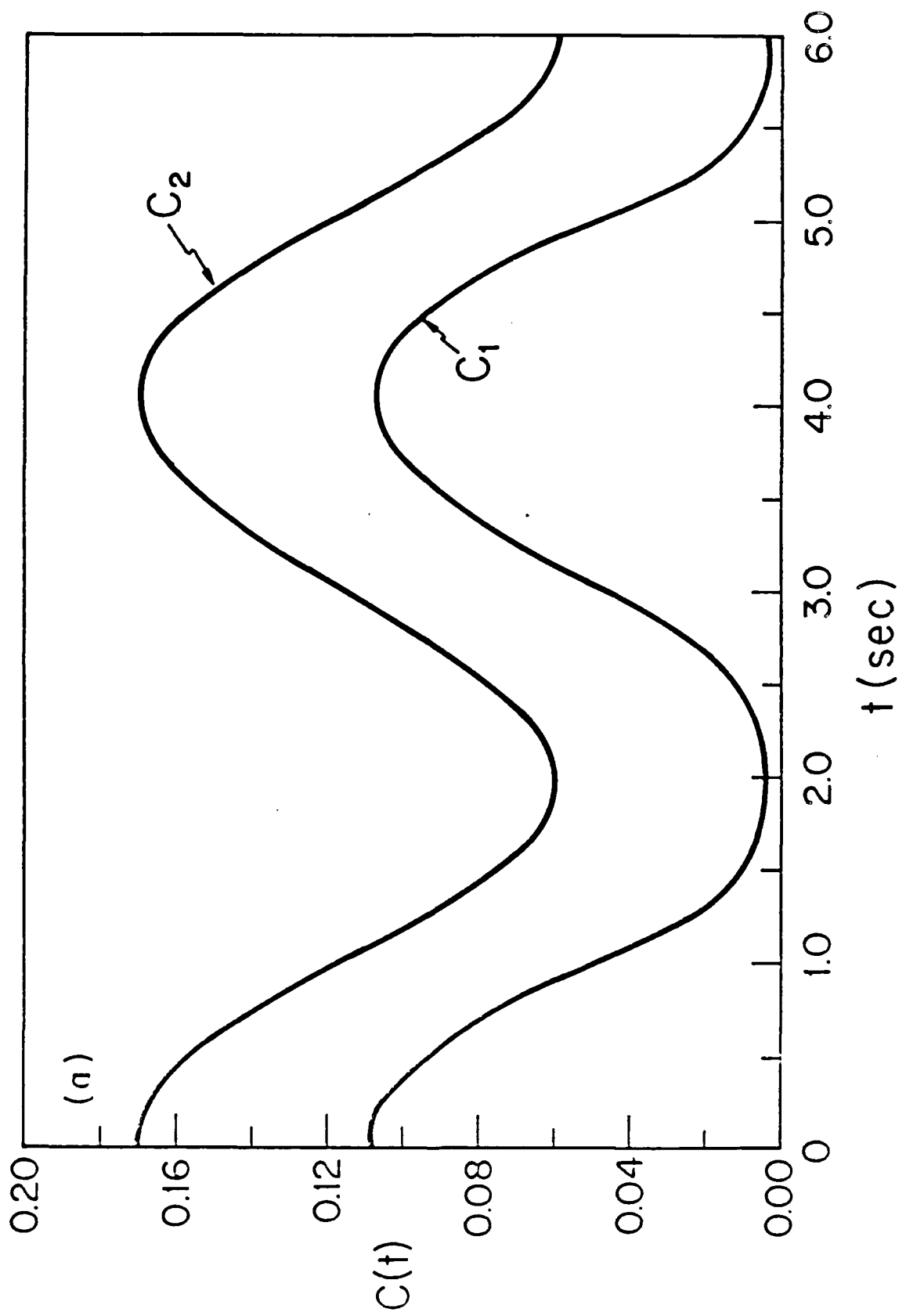


Figure 6

Typical concentration traces obtained by the ensemble averaging technique. Subscripts refer to measurement locations indicated in Figure 1. (a) Concentration traces for $\beta = 1.52$, $Pe = 31.2$. (b) Concentration traces for $\beta = 4.81$, $Pe = 2.35$.



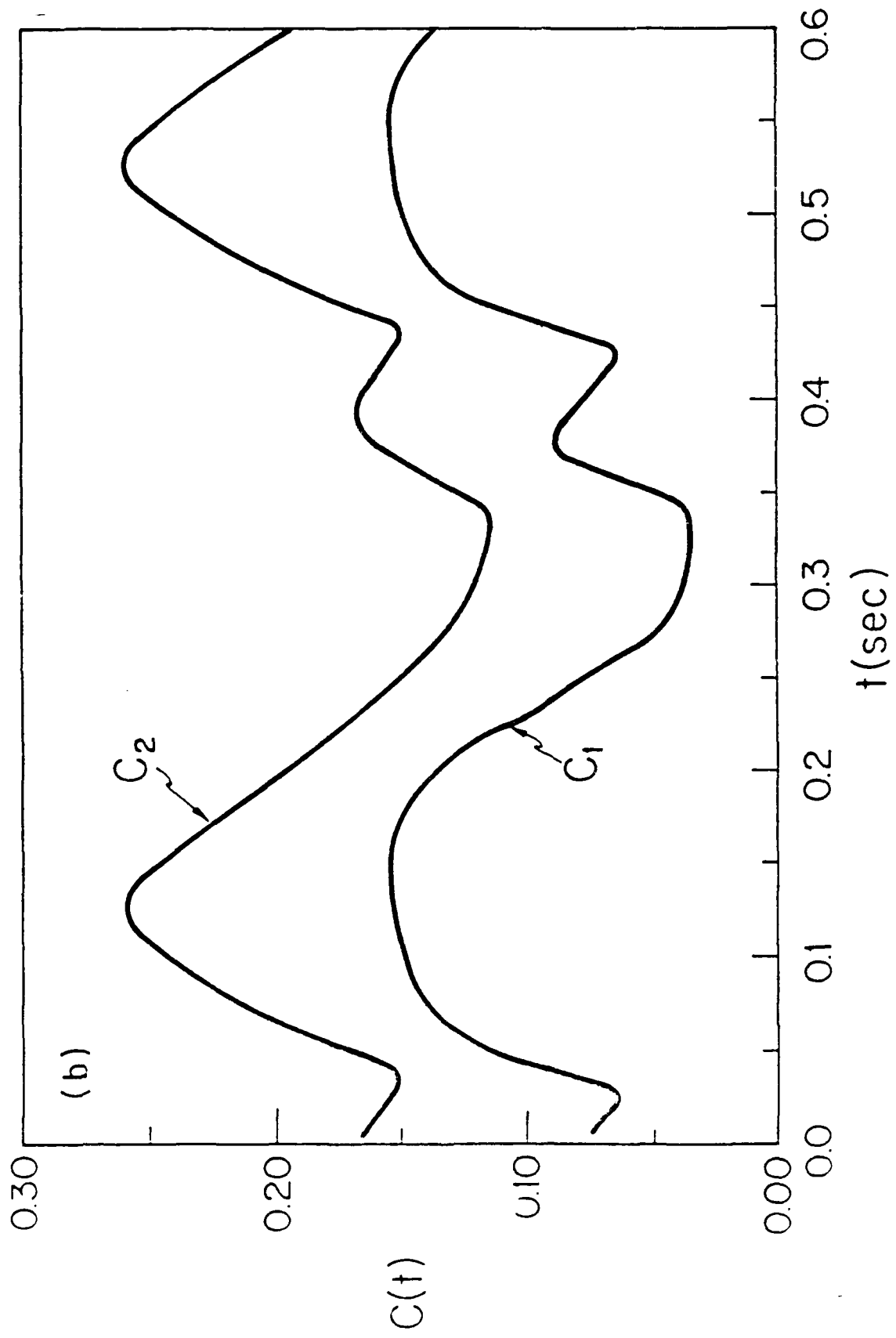


Figure 7

Comparison of all experimental data to the regression
formula $D = 0.078 Pe^{1.66} \beta^{-1.45}$.

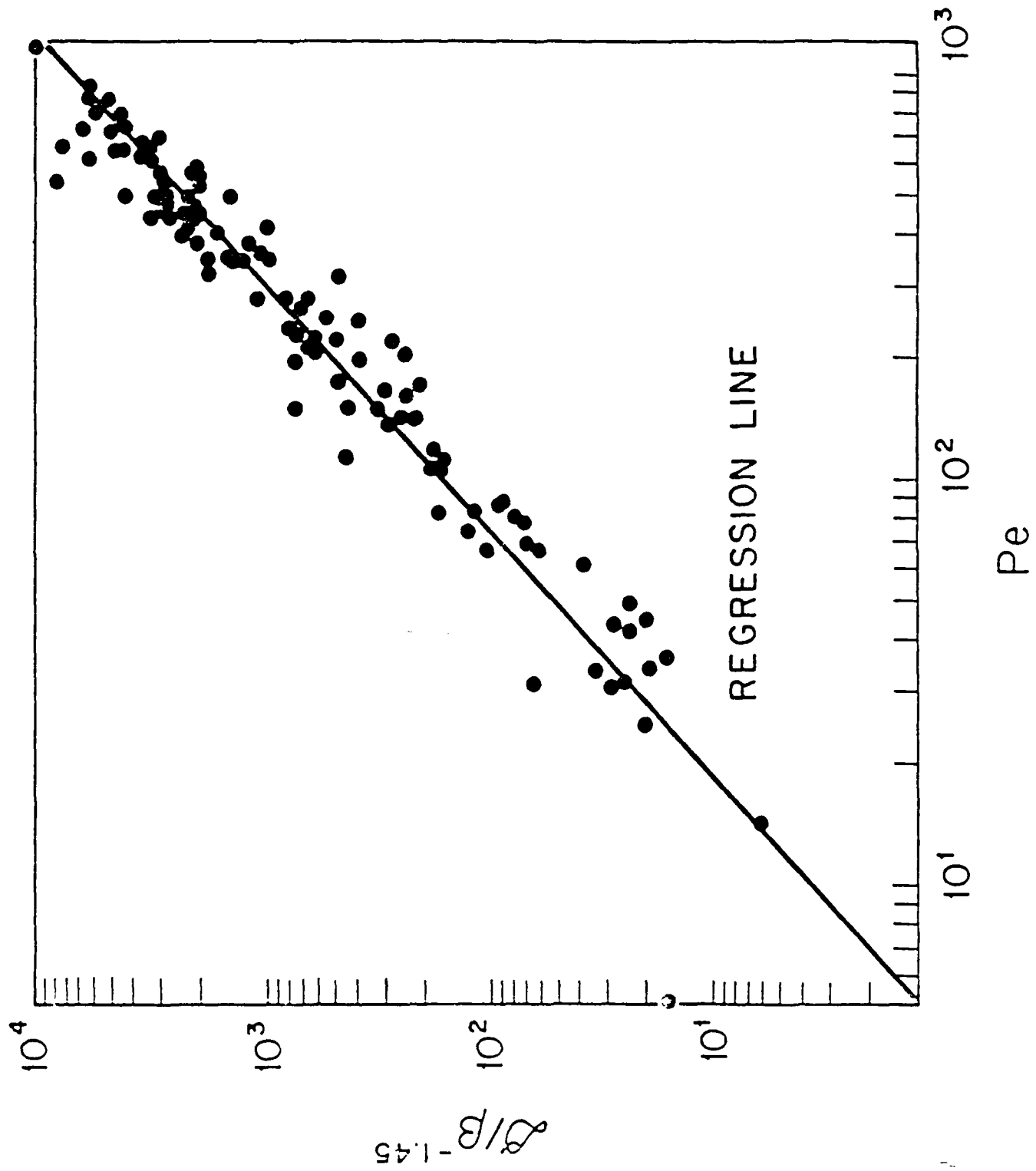


Figure 8

A comparison of our results for series A and B to the theoretical prediction for a straight tube with sinusoidal flow (solid line). 82% of the data fall within the shaded zone.

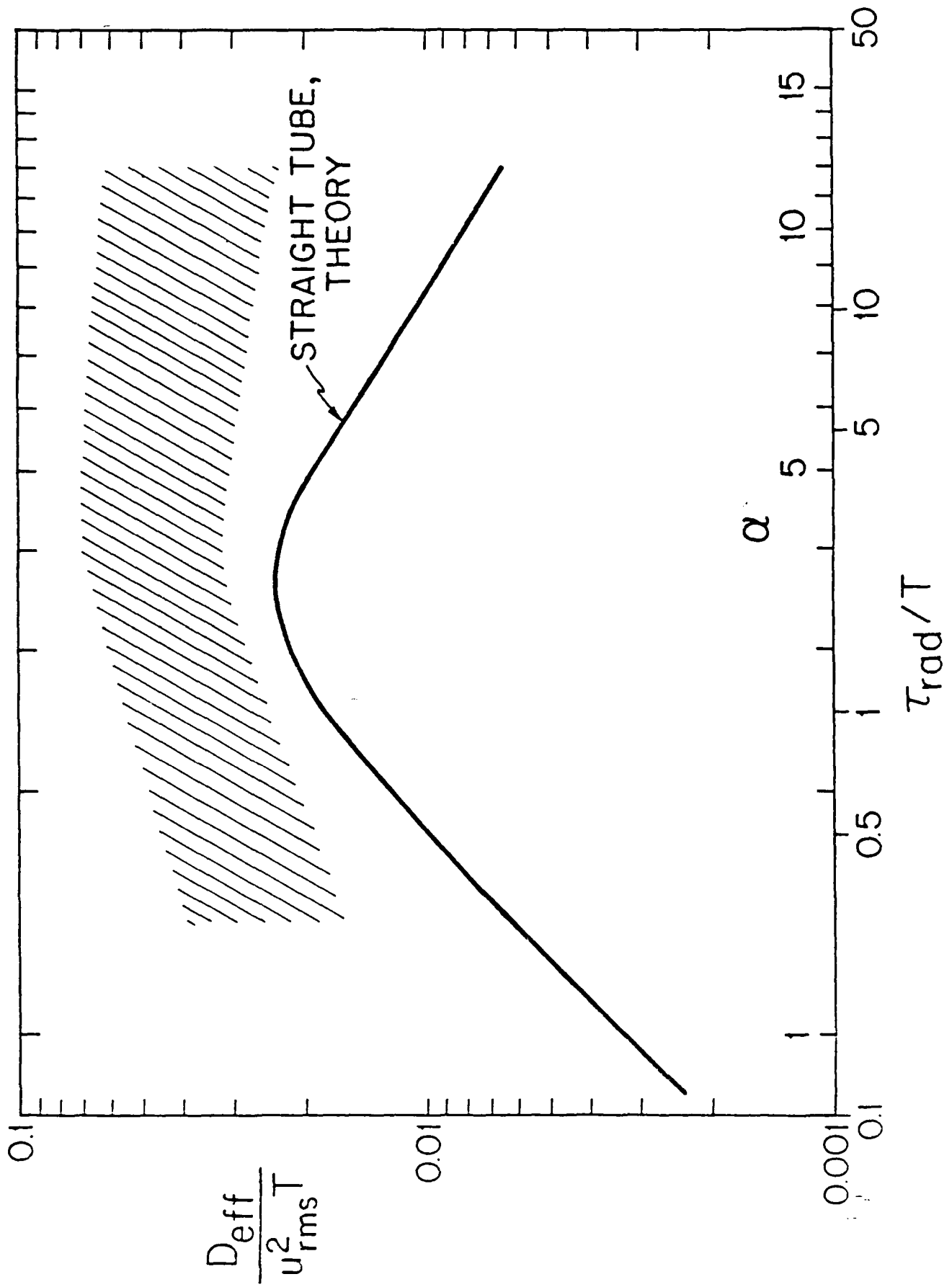


Figure 9

Data correlations found in experiments conducted in branching networks. Steady flow in gases - solid line (Scherer et al, 1975): oscillatory flow in liquids - dashed lines that bracket the range $4 < \beta < 10$ (Tarbell et al, 1982): and oscillatory flow in gases - dash-dot line that bracket the range $4 < \beta < 10$ (both series A and B for this study). Correlations are plotted only for the range of parameters common for all experiments. See text for a description of the comparison.

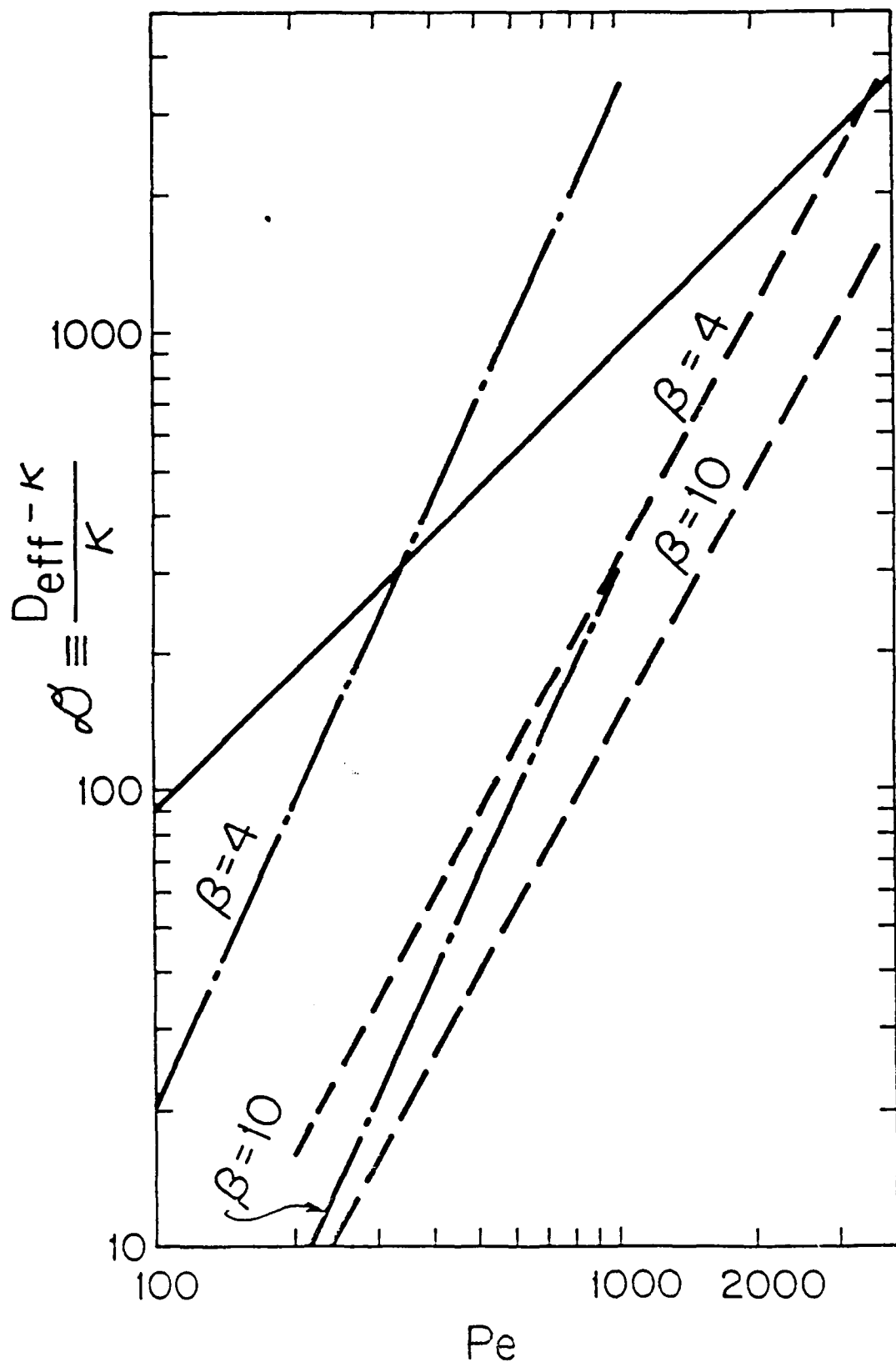


Table 1. Data Correlations.
Coefficients are provided below for two general expressions:

Generation	Frequency range	\bar{q}	\bar{r}	\bar{s}	\bar{q}	\bar{r}	\bar{s}	Mean & error
1	$\beta < 4$	0.114	1.41	-0.981	0.549	1.41	0.915	19.2
1	$\beta > 4$	0.034	2.13	-2.47	0.305	2.13	0.891	6.91
1	all data	0.155	2.10	-2.02	0.214	2.10	1.09	16.8
2	all data	0.208	1.47	-1.26	0.913	1.47	0.840	36.2
1 and 2	all data	0.078	1.66	-1.45	0.508	1.66	0.940	31.5

(a) computed from the expression $(\sum_{i=1}^N D_{eff,i} - D_i) / N$ where D_i is the correlation value, $D_{eff,i}$ is the corresponding data value, and N is the total number of data points in the correlation.

END

DATE

FILMED

DTIC

July 88